Published in final edited form as:
Inorg Chem. 2010 April 19; 49(8): 3573–3583. doi:10.1021/ic901814f.

Transition Metal Ions in Zeolites: Coordination and activation of O_2

Pieter J. Smeets[1,2], **Julia S. Woertink**[2], **Bert F. Sels**[1], **Edward I. Solomon**[2,3], and **Robert A. Schoonheydt**[1,*]

[1] Center for Surface Chemistry and Catalysis, K.U.Leuven, Kasteelpark Arenberg 23, 3001 Leuven, Belgium.

[2] Department of Chemistry, Stanford University, Stanford, CA 94305, USA

[3] Stanford Synchrotron Radiation Lab, Menlo Park, CA 94025, USA

Abstract

Zeolites containing transition metal ions (TMI) often show promising activity as heterogeneous catalysts in pollution abatement and selective oxidation reactions. In this paper, two aspects of research on the TMI Cu, Co and Fe in zeolites are discussed: (i) coordination to the lattice and (ii) activated oxygen species. At low loading, TMI preferably occupy exchange sites in six-membered oxygen rings (6MR) where the TMI preferentially coordinate with the oxygen atoms of Al tetrahedra. High TMI loadings result in a variety of TMI species formed at the zeolite surface. Removal of the extra-lattice oxygens during high temperature pretreatments can result in auto-reduction. Oxidation of reduced TMI sites often results in the formation of highly reactive oxygen species. In Cu-ZSM-5, calcination with O_2 results in the formation of a species, which was found to be a crucial intermediate in both the direct decomposition of NO and N_2O and the selective oxidation of methane into methanol. An activated oxygen species, called α-oxygen, is formed in Fe-ZSM5 and reported to be the active site in the partial oxidation of methane and benzene into methanol and phenol, respectively. However, this reactive α-oxygen can only be formed with N_2O, not with O_2. O_2 activated Co intermediates in Faujasite (FAU) zeolites can selectively oxidize α-pinene and epoxidize styrene. In Co-FAU, Co^{III} superoxo and peroxo complexes are suggested to be the active cores, whereas in Cu and Fe-ZSM-5 various monomeric and dimeric sites have been proposed, but no consensus has been obtained. Very recently, the active site in Cu-ZSM-5 was identified as a bent $[Cu\text{-}O\text{-}Cu]^{2+}$ core (*Proc. Natl. Acad. Sci. USA* **2009**, 106, 18908-18913). Overall, O_2 activation depends on the interplay of structural factors such as type of zeolite, size of the channels and cages and chemical factors such as Si/Al ratio and the nature, charge and distribution of the charge balancing cations. The presence of several different TMI sites hinders the direct study of the spectroscopic features of the active site. Spectroscopic techniques capable of selectively probing these sites, even if they only constitute a minor fraction of the total amount of TMI sites, are thus required. Fundamental knowledge of the geometric and electronic structure of the reactive active site can help in the design of novel selective oxidation catalysts.

1. Introduction

The interaction of O_2 with the surface atoms in the micropores and channels of zeolites has been studied since the 1960's. It was recognized at that time that the adsorption enthalpy of N_2 in zeolite A (LTA, Figure 1A) was systematically higher than that of O_2, because of the

* Corresponding author: Center for Surface Chemistry and Catalysis, K.U.Leuven, Kasteelpark Arenberg 23, 3001 Leuven, Belgium. Robert.schoonheydt@biw.kuleuven.be; tel.: +32-16-321610. .

quadrupolar moment of N_2. The pressure-swing-adsorption (PSA) process was developed to separate O_2 and N_2 from air on an industrial scale.[1-6] The adsorption enthalpy of O_2 at zero coverage is 15-20 kJ/mol. The adsorbed molecule is coordinated end-on to the exchangeable cations, thus making the infrared (IR) inactive stretching vibration of O_2 active. The measured values range from 1555 – 1552 cm^{-1} for alkali and alkaline earth exchanged zeolites, slightly below the 1556 cm^{-1} measured by Raman spectroscopy for gaseous O_2.[7-9] However, for the O_2 in interaction with Cu^+ in FAU, O=O stretching vibrations at 1256 and 1180 cm^{-1} were recently measured.[10] These were ascribed to O_2 interacting with Cu^+ in sites II and III of the FAU framework, respectively (See Figure 1B). This red shift points to a significant weakening of the O=O bond due to electron transfer from Cu^+ to the π^* antibonding orbitals of O_2.

Such an electron transfer was already observed in the 1970's by Klier and coworkers in zeolite A loaded with TMI.[11-14] Thus, Cr(II)-A reversibly adsorbs one O_2 per Cr(II) at room temperature (RT). The spectral changes point to the reaction:

$$Cr^{2+} + O_2 \leftrightarrow Cr^{3+} - O_2^-$$

And similarly for Cu^+:

$$Cu^+ + O_2 \leftrightarrow Cu^{2+} - O_2^-$$

Fe^{2+} in zeolite A does not bind O_2 at RT, but upon heating in O_2 Fe^{2+} is oxidized to Fe^{3+} and the formation of a Fe^{3+} -O- Fe^{3+} species was suggested.[14]

At about the same time Lunsford and coworkers prepared faujasite-type zeolites (Figure 1B) loaded with amine complexes of Cu^{2+} and Co^{2+}.[15, 16] The Co-amine complexes take up O_2 at RT to form the corresponding mononuclear superoxo complexes, identified by their characteristic UV-VIS and EPR spectra. These mononuclear superoxo complexes were unstable due to their mobility in the zeolitic cavities and evolved slowly into dinuclear peroxo complexes.[17, 18] Later on, bulky Co complexes were synthesized in the supercages of zeolite Y. These complexes were trapped in the supercages and could not diffuse through the zeolitic cavity system. Upon interaction with O_2 stable mononuclear superoxo complexes were obtained.[18]

In the search for new and improved heterogeneous catalysts for pollution abatement and selective oxidation, research was redirected to TMI in mordenite (MOR) and MFI-type zeolites (Figure 1C and D), with ZSM-5 (a zeolite with MFI topology) as the most prominent example. In this paper we discuss the activation of O_2 by TMI in these zeolite topologies with special emphasis on selective oxidation of hydrocarbons and catalytic decomposition of N_2O and NO into N_2 and O_2. After a short introduction on the fundamentals of zeolite structures, this contribution presents an overview on the present state of knowledge of the coordination of TMI with surface oxygen. Several excellent reviews have been published on the catalytic oxidation of organic substrates by TMI in zeolites or on other supports.[19-24] In this paper we will focus mainly on the first row transition metals Cu, Fe and Co in zeolites. As some of these coordinated TMI are able to activate O_2 or N_2O under moderate conditions, understanding their geometric and electronic structures might lead to the development of novel active and selective oxidation catalysts.

2. Zeolites

Zeolites are three-dimensional microporous silicates. The primary building unit is the $[SiO_4]^{-4}$ tetrahedron. It forms a three-dimensional network by corner-sharing of the 4 oxygen atoms and leads to charge neutral network.[1, 25] Due to the crystalline ordering, zeolites contain ordered pores and cavities that have characteristic shapes and sizes. 176 different structure types are known.[26] Some of these can be found in nature as minerals, but most are synthetic materials. Corner sharing and strictly alternating negatively charged Al and positively charged P tetrahedra, $[AlO_4]^{-5}$ and $[PO_4]^{-3}$, can also be used as primary tetrahedral units. They give the so-called crystalline, microporous AlPO materials. Some of them are isostructural with the silicates, others do not have a siliceous counterpart. Zeolites are represented with three letters codes, that are under the supervision of the structure commission of the International Zeolite Association (IZA).[26, 27]

Isomorphous substitution is the replacement of a cation in the lattice by another cation with approximately the same size but with different charge. The most important is the substitution of Si^{4+} by Al^{3+}, thus giving an overall negative charge to the framework. This charge is neutralized by exchangeable cations, located in the channels or cages of the structure. The amount of exchangeable cations is expressed by the cation exchange capacity (CEC). In principle the degree of Al for Si substitution ranges from zero (Si/Al = infinity) to Si/Al = 1. Whatever the Si/Al ratio, the isomorphous substitution obeys Loewenstein's rule: two Al tetrahedra cannot be neighbors sharing an oxygen atom.[1] Thus, an Al tetrahedron must share its 4 oxygens with 4 Si tetrahedra, and with Si/Al = 1 a strict alternation of Si- and Al-tetrahedra occurs in the structure. Such is the case for zeolite A (LTA).

In industrial applications the most important zeolites are Linde Type A zeolite (LTA), FAU, MFI and MOR. Their idealized structures are shown in Figure 1. Table 1 summarizes their unit cell dimensions and typical sizes of their channels/cages. The dimensions of the zeolite pores allow for separation of molecules on the basis of their sizes, the so-called molecular sieving effect. In catalysis this property is often referred to as shape selectivity.[25] An example is the cracking of alkanes in acid MFI-type zeolites. Here the zeolite pores allow only the linear molecules to enter the pores containing the acid sites that regulate the cracking. Branched molecules are excluded from the pores and hence do not react.[28]

Another area of zeolite research is the immobilization of homogeneous catalysts. In FAU zeolites for instance, TMI complexes exchanged in the supercages are readily accessible for reagents (unlike the TMI exchanged in the sodalite cages,[29] that are only accessible through a 6MR). After reaction, a simple filtration suffices to separate the catalyst from the reaction products. This separation is often problematic in the case of homogeneous catalysts. As an example, superoxo and peroxo complexes have been obtained in the supercages of zeolite Y by interaction of O_2 with cobalt-amine complexes, immobilized in the supercages of zeolite Y.[18] There are several ways to synthesize these complexes in the supercages, the preferred procedure depending on the type of complex. If the complexes are stable under exchange conditions, cationic and smaller than the free diameter of the 12 membered ring (MR) giving access to the supercages, they can be exchanged from aqueous solution. Other syntheses involve the adsorption of appropriate ligands in the zeolite, pre-exchanged with TMI, or the complexes can be synthesized in situ e.g. in the supercages of FAU-type zeolites.[18, 19, 30]

TMI can in principle substitute for Si^{4+} or Al^{3+} in the zeolitic structures during synthesis, resulting in a zeolite lattice containing TMI. Parameters to be taken into account are: (i) size and charge of the TMI; (ii) pH of the synthesis medium; (iii) the ability of the TMI to adopt tetrahedral coordination with oxygen atoms. In most cases, the amount of TMI incorporated in the lattice by hydrothermal synthesis is very limited. The two most common examples are

Ti^{4+} and Fe^{3+}. Ti^{4+} exchanged in silicalite for instance is called TS-1 and is found to be an active catalyst in converting benzene with hydrogen peroxide into phenol.[31-33] Fe^{3+} in the lattice is often due to the presence of impurity in zeolite synthesis, but it can also be added as a reagent into the synthesis mixture. One of the problems with TMI in the lattice is thermal stability. Upon high temperature treatment, some of the TMI in the structure are extracted and found as so-called extra-lattice TMI, which can be monomeric, dimeric or appear as oligomers.[34] All of them are possible catalytic sites.

Aqueous ion exchange is the most commonly used method for preparing zeolites with TMI located at exchange sites. The resulting material contains aqueous TMI in the pores and cavities of the zeolite. Upon high temperature treatment water is removed and the TMI coordinates to surface oxygens of the exchange sites. These sites have been compiled by Mortier a long time ago.[35] They are crystallographically well defined in the case of zeolites with low Si/Al ratios such as LTA, FAU and MOR (Figure 1). This is much less so for zeolites with high Si/Al ratios such as MFI.

As aqueous solutions of TMI can be acidic, the exchange reaction can be accompanied by side reactions such as the exchange of protons and partial lattice destruction. To avoid these side effects other exchange techniques have been developed, including solid state exchange,[36-38] or simply buffering the aqueous solution.[39, 40]

3. Coordination of TMI in zeolite channels and cages

As mentioned above, isomorphous substitution of Al^{3+} for Si^{4+} renders the zeolite framework negatively charged. This negative charge is compensated by extra-framework cations located in the pores or cages of the zeolite. As these cations are not part of the framework, they can be exchanged by other cations, in particular TMI. The actual location depends on several factors among which are the Si/Al ratio, the total amount of TMI, charge of the TMI, exchange method and conditions (pH and temperature being the most important).

Initially, the TMI will occupy the most favorable exchange sites and try to maximize their coordination number. In FAU for instance, after dehydration, the TMI are preferably located inside the hexagonal prisms (sites I, Figure 1B) and in the sodalite cages (sites I′, Figure 1B). At higher loadings, the more accessible exchange sites in the supercages (accessible through 12 membered oxygen rings (12MR)) are occupied (sites II and III, Figure 1B). Among these sites, sites I′ and II are the most important. Both are six-membered oxygen rings (6MR). In MFI, TMI are located in the ten-membered ring (10MR) channels or at channel intersections. They are coordinated to six-membered rings containing one or two Al tetrahedra, but 5MR with one Al cannot be excluded. The same holds for MOR with its 12MR and 8MR channel system.[35]

TMI coordinated to the zeolite lattice have typical spectroscopic signatures, i.e. d-d transitions and EPR spectra. These spectra are usually reasonably resolved at low loadings of TMI. In the work of Wichterlova and co-workers,[41-46] three exchange sites are discerned for Co ions in pentasil zeolites and Beta (*BEA), denoted as α, σ and γ sites. In Figure 2A, an overview of these sites is shown and their location in ZSM-5 is given in Figure 2B. Co^{2+} exchanged into one of these sites results in a characteristic set of d-d transitions in the UV-vis spectrum as shown in Table 2. Using chemometric techniques Verberckmoes et al. identified three different types of coordination sites for Co^{2+} in LTA and FAU zeolites from their ligand field absorption spectrum: trigonal and pseudo-tetrahedra sites in site I′, II and II′ and a pseudo-octahedral in site I (only in FAU) (Figure 1).[47, 48]

In the work of Schoonheydt and co-workers,[49-54] a set of Cu-containing zeolites was studied with UV-vis-NIR absorption and EPR spectroscopies. Examples of EPR spectra are shown in

Figure 3, and the d-d transitions and EPR parameters of these Cu^{2+} sites are summarized in Table 3. For Cu^{2+} in FAU and LTA, 3 d-d transitions are resolved with the most intense band in the region 10500 – 11000 cm^{-1} and two weaker bands around 12500 cm^{-1} and 15000 cm^{-1}. The corresponding EPR spectra reveal two signals, one with g_{ll} = 2.37-2.41 common for LTA and FAU and one with g_{ll} = 2.30-2.34, not found in LTA. For MOR and MFI the d-d transitions occur at higher energies and overlap such that only a broad band is observed at around 14000 cm^{-1}. This d-d spectrum is accompanied by 2 EPR signals with characteristic g_{ll} values of 2.30-2.33 and 2.26-2.28. The $g_{\perp}$ values are all situated in the 2.09 - 2.05 range but the hyperfine splitting in the perpendicular region is not well resolved.

These spectra have traditionally been interpreted in terms of Cu^{2+} coordinating the 6MR's in a trigonal configuration (C_{3v}). The two EPR signals are then ascribed to 6MR's in different crystallographic positions, such as sites I′ and II in FAU (Figure 1B), irrespective of the number of Al tetrahedra making up the 6MR's. A ligand field analysis of the d-d transitions of Co^{2+} and Cu^{2+} in six-ring sites indicated that the TMI are not symmetrically coordinated in the center of the ring, but undergo an off-axial displacement.[55-58] Detailed ab initio quantum-chemical analysis revealed that coordination of Cu^{2+} or Co^{2+} in a specific exchange site leads to a strong site distortion.[49, 51-54] First, the TMI try to maximize their coordination number. Second, the oxygens of the Al tetrahedra are preferentially coordinated to the TMI. This leads to site distortion and the TMI is not located exactly in the center of the 6MR. This is shown in Figure 4 for Cu^{2+} coordinated to lattice O atoms in the α, β and γ site in ZSM-5. This distortion depends on the number of Al tetrahedra making up the coordination site. Thus, a TMI in one crystallographic exchange site can have several spectroscopic signatures, depending on the number of Al tetrahedra. All these studies taken together lead to the conclusion that both the crystallographic position of the exchange site and the number of Al tetrahedra making up the site determine the spectroscopic signatures of the TMI in that site (see Figure 4).

At high TMI loading, additional less energetically favorable exchange sites are occupied providing fewer coordination bonds to lattice O-atoms. The spectroscopic signatures of TMI in these sites are much less resolved since at high TMI loadings various TMI species can co-exist: mononuclear, di- and oligonuclear clusters up to chains of TMI. Often, the classical techniques used to characterize TMI in zeolites, such as UV-vis absorption, EPR, XRD and EXAFS give averages of overlaying spectra. At higher TMI loadings, some of the paramagnetic TMI might be EPR silent due to anti-ferromagnetic coupling and dipolar broadening, and subtle changes in the ligand field of TMI at various sites result in the formation of overlapped unresolved absorption features. Further, EXAFS gives spectra which are a superposition from TMI in different sites. Thus it is extremely difficult to distinguish the contributions of a specific TMI site.

TMI sites can act as catalytic centers if they have open coordination sites and if they are readily accessible for guest molecules. In FAU zeolites, 6MR's separate the sodalite cages from the supercages, and as a result the TMI located inside the sodalite cages are inaccessible to molecules, which cannot diffuse through the 6MR with a free diameter of ~0.23 nm. In MFI, TMI are located in the straight or zigzag 10MR channels which have a free diameter of −0.55 nm. These are the only sites that can contribute to the overall catalytic activity. Similar considerations can be made for other zeolites: the smaller the pores, the less accessible the sites. In addition, larger pores allow for faster diffusion of reagents to the active sites inside the zeolite crystals and for the efficient release of reaction products out of the zeolite crystals, thereby: i) liberating the active site faster for a second reaction, and ii) decreasing the probability of unwanted side reactions, thus increasing the selectivity.

TMI-loaded zeolites such as Co^{3+}, Fe^{3+} and Cu^{2+} can undergo auto-reduction during high temperature pretreatment in He or vacuum. The auto-reduction of Fe^{3+} to Fe^{2+} during He

treatments is reported[60-63] and confirmed by L and K edge XAS measurements.[64-67] It was attributed to the dehydration and desorption of O_2 from two $Fe^{3+}(OH)_2$ sites leaving two $Fe^{2+}(OH)$ species.[62, 68] In Cu-zeolites, it has been reported that this auto-reduction can be achieved by dehydration of two $Cu^{2+}(OH)$ sites, resulting in a Cu^+ and a Cu^{2+}-O^- site[69] or a bridged binuclear Cu^{2+} site. In the latter case desorption of O_2 gives two Cu^+.[70]In Cu-FAU, the auto-reduction was suggested to involve the formation of "$[AlO]^+$" Lewis acid sites as first described by Jacobs and Beyer,[71] although the former process was also suggested. This auto-reduction for Cu-zeolites is confirmed by XAFS spectroscopy, showing a reduction of the number of O atoms constituting the first coordination shell and the observation of a feature at 8983 eV in the XANES spectra,[72] assigned as the 1s → 4p transition in Cu^+.[73] In addition, monovalent copper in MFI is characterized by 2 typical luminescence bands around 470-490 nm and 520-540 nm, assigned to transitions from the $3d^94s^1$ triplet state to the $3d^{10}$ singlet ground state.[74-76] The 480 nm band is assigned to Cu^+ coordinated to 3-4 oxygens of the 6MR in the sinusoidal channels of ZSM-5. The 540 nm emission is attributed to Cu^+ coordinated to 2 oxygen atoms at channel intersections. As for Cu^{2+}, the preferred oxygen atoms in the coordination sphere of Cu^+ are those of the Si-O-Al bridges. What is still unclear is whether the sites of Cu^+ are the same as those of Cu^{2+}, in other words, whether or not the reduction of divalent copper is accompanied by a migration of Cu^+ to a new coordination site.

4. Activated oxygen on TMI and its reactivity

4.1 Cu-zeolites

Auto-reduction is a crucial step in the catalytic decomposition of NO and N_2O into N_2 and O_2 over Cuzeolite catalysts. Indeed, the oxygen atoms of N_2O and NO are deposited on Cu^+ with release of N_2 and N_2O respectively. In the rate limiting step, these deposited oxygen atoms recombine and desorb as molecular oxygen.[29, 72, 77-80] The closer the deposited O species are located to each other, the faster is the recombination. This is shown in Figure 5 for the N_2O decomposition over a range of Cu-exchanged zeolites. Here the amount of EPR-silent Cu^{2+} is used as a measure of the average Cu-Cu distance, as Cu^{2+} becomes EPR-inactive due to anti-ferromagnetic coupling or dipolar broadening between closely located Cu^{2+} cores. A smooth increase of the N_2O decomposition activity with the amount of EPR-silent Cu has been observed in MOR, FER, and BEA catalysts.[80] Notably, Cu-ZSM-5 shows a much higher activity for decomposing N_2O, as can be seen in Figure 5. Clearly, a special type of active site must be present in ZSM-5. A similar trend was observed in the decomposition of NO. Cu- rich ZSM-5 samples (with Cu/Al>0.2) show much higher activity compared to other Cu-zeolites. In the work of Schoonheydt and coworkers, this was attributed to the presence of an unique Cu core with a characteristic absorption feature around 22 700 cm^{-1}, which was detected by *in situ* UV-VIS absorption spectroscopy during catalytic decomposition of NO and N_2O.[77, 80]

Interestingly, a similar absorption band was also observed after contacting Cu-ZSM-5 catalysts with high Cu/Al ratios (Cu/Al>0.25) with O_2 at elevated temperatures.[72, 81] As dioxygen is consumed in the process, the unique absorption may tentatively be assigned to an O-activated Cu species. Moreover, the active oxygen was found to selectively oxidize methane into methanol in a stoichiometric reaction, starting at 100°C (Figure 6).[81, 82] During the reaction with CH_4, the 22 700 cm^{-1} band disappears, indicating that the active Cu core in ZSM-5 is involved in both the catalytic decomposition of nitrogen oxides and the selective oxidation of methane.[77, 80] The nature of the active Cu core was investigated in a combined UV-vis, EPR and EXAFS study and the obtained data were suggested to be consistent with a bis(μ-oxo) dicopper(III) core.[72, 77] The energy of the absorption band and the Cu-Cu distance of 2.87 Å obtained by EXAFS were used to rule out the presence of a peroxo moiety which typically has longer Cu-Cu distances.[83] From the amount of methanol produced, the number of active Cu centers was estimated to be approximately 5% of the total amount of Cu in Cu-ZSM-5, i.e. the

species associated with the 22 700 cm^{-1} is a minority species.[81, 82] As EXAFS shows the averaged data for all Cu sites in Cu-ZSM-5, it is not sensitive enough to probe these active Cu sites. As several Cu-oxygen species show absorption features in this region,[84-90] no conclusive assignment can be made based on the UV-vis electronic absorption data alone.

Several DFT studies evaluated the possible binuclear Cu species formed in Cu-ZSM-5 upon calcination in O_2. From the calculations of Yumura *et al*. both side-on peroxo and bis(μ-oxo) dicopper cores were found to be energetically favorable in the 10MR of ZSM-5.[91] In the work of Goodman *et al*. and Bell and co-workers, several oxygen bridged binuclear Cu sites were proposed.[92-94] In the work of Iwamoto *et al*.,[95] and later others,[96-100] an oxygen bridged Cu dimer was suggested to be formed during the auto-reduction of two hydrated Cu^{2+} cores. Aside from a Cu-Cu contribution in EXAFS data, no other spectroscopic evidence for such a core with bridging oxygen was presented to support the assignment. Computational studies have evaluated several possible core structures. Direct spectroscopic data are required that can selectively probe the active site, even if it is only a minority species. In fact, we have recently used the 22 700 cm^{-1} absorption band to resonance enhance the Raman vibrations of the catalytic site upon shooting a laser in this absorption band. In these studies the reactive intermediate is unambiguously defined as a bent $[Cu\text{-}O\text{-}Cu]^{2+}$ core, a species not previously observed in Cu/O_2 chemistry, as the catalytically active species. The details of these spectroscopic studies and the frontier orbitals involved in H-atom abstraction from CH_4 are presented in reference [101].

In addition to this Cu core in Cu-ZSM-5, other Cu sites are capable of stoichiometric oxidation of methane in methanol.[82] In Cu-MOR a similar absorption feature at 22 000 cm^{-1} was observed after O_2 calcination, although much less intense than that of Cu-ZSM-5. This band also disappeared during reaction with CH_4 at 150°C, and methanol was produced. Less active Cu cores were formed in FER and BEA. Here, a reaction temperature of 200°C is required to convert methane into methanol. In MOR, the amount of methanol produced after reaction at 200°C significantly increased, compared to the reaction at 150°C, indicating the presence of an additional core. Thus, while an activated Cu species, corresponding to the 22 700 cm^{-1} absorption band in ZSM-5 and MOR is capable of oxidizing CH_4 at 100°C, another less active but unknown Cu species is present in the FER, BEA and MOR zeolites, that is capable of only oxidizing methane above 200°C.[82]

4.2 Fe-zeolites

Panov and co-workers reported the formation of the so-called α-O core in Fe-ZSM-5 upon reacting the zeolite with N_2O,[102-104] suggested to mimic the selective hydroxylation of methane into methanol by the enzyme sMMO.[105-107] High temperature treatment in He, vacuum, H_2 or steam generates the precursor for this α-O core and is referred to as α-Fe.[108-113] Subsequent reaction of the Fe-zeolite with N_2O at temperatures between 200 and 250°C results in the formation of α-O, a site capable of selectively oxidizing methane to methanol and benzene to phenol at room temperature. There is consensus that this active site cannot be formed with O_2.[114-116] Several studies address the comparison and differences between α-O and the active site in sMMO.[61, 110, 117, 118] In the past decades, a number of structural assignments, often contradictory, have been made for the α-O and α-Fe sites and no consensus as to its structure has been attained thus far. Part of the controversy is due to the lack of a direct correlation between the reported spectroscopic data to the reactivity of these sites in the oxidation of CH_4 or benzene. Based on Mössbauer spectroscopy and EXAFS data, the core was originally assigned to a bis(μ-oxo)diiron core, in analogy with the active site in sMMO.[107] Later work suggested the formation of a Fe^{4+}=O intermediate[61, 119] or alternatively a $Fe^{3+}O^{\cdot -}$ radical[120, 121] or two $Fe^{3+}O^{\cdot -}$ μ-OH bridged sites.[113] The formation of an $Fe^{3+}O^{\cdot -}$ radical was tentatively suggested, based on the co-existence of signals at g=6.4 and g=2.018

in the EPR spectrum, assigned to Fe^{3+} and an $O^{\cdot -}$ radical moiety, respectively.[122] However, if an Fe^{3+}-$O^{-\cdot}$ core exists, the S=5/2 of Fe^{3+} should couple antiferromagnetically with the radical S=1/2, resulting in an overall S=2 ground state, which would not be detectable by X-band EPR spectroscopy at liquid N_2 temperatures.[123-125] Fe^{4+}=O was ruled out since it would not contribute to the EPR spectrum at liquid N_2 temperatures. However, the total amount of spin observed was not quantified with respect to the total Fe content. Thus it is not possible to judge whether the presence of EPR silent Fe centers, such as a Fe^{4+}=O, can be excluded. Assigning these EPR features to the active site was based on their disappearance after interaction with CO at room temperature, but the more direct approach of measuring the EPR spectra after reaction with CH_4, was not pursued. In combination with the above mentioned EPR study, X-ray absorption data were collected and presented as inconsistent with an Fe^{4+} species.[120, 121, 126] However, these bulk techniques do not rule out the presence of a minor amount of catalytic Fe^{4+} in the presence of a large fraction of spectator sites. Thus no data exist that can unambiguously evaluate for the presence or absence of an Fe^{4+} core or relate it to the reactive α-O species. Recently, attempts have been undertaken to investigate the α-O site with UV-vis absorption and resonance Raman spectroscopy by Li and coworkers,[127] and the α-site was tentatively assigned as a peroxo bridged binuclear Fe site, based on the observation of a stretch at 867 cm^{-1} and an electronic absorption band at 605 nm (16500 cm^{-1}).

Formation of this α-O and the subsequent hydroxylation of CH_4 and benzene, could only be achieved after deposition of an O atom from N_2O, but not after reaction with O_2. Treatment of Fe-ZSM-5 with O_2 was studied in the work of Sachtler and co-workers.[128] In their Raman study, an adsorbed peroxide species was suggested to be formed bridging two Fe^{3+} centers. The presence of a peroxo intermediate was concluded based on a Raman feature at 730 cm^{-1} assigned as the O-O stretching vibration. Distinguishing vibrations involving O motions can be made upon ^{18}O isotopic labeling, as these vibrations shift to lower frequencies. The work of Sachtler and co-workers shows a red shift of 32 cm^{-1} to 698 cm^{-1} when the Fe-ZSM-5 is reated with $^{18}O_2$ confirming the involvement of extra-lattice O motion in the Fe complex. In Fe-zeolites, the presence of Fe dimers is suggested to be reflected by the presence of an absorption band in the 28 000-30 000 cm^{-1} region,[129] but this assignment is debated.[126] Interestingly however, a peroxo bridged Fe^{3+} dimer is suggested in the work of Sachtler as well as in the work of Li and co-workers, although the suggested peroxo stretches at 730 cm^{-1} and 867 cm^{-1} are very different.[127, 128] More detailed spectroscopic investigation is thus required to further unravel the geometric and electronic structures of the oxygen bridged Fe dimers suggested to be formed from O_2 and N_2O. If it is in fact the case that both N_2O and O_2 treatments result in peroxo bridged Fe dimers, as suggested by Li and Sachtler respectively, it is important to understand how the different geometric and electronic structures (resulting in different peroxo stretches) contribute to their different reactivities. Only the N_2O-activated form, the α-O (which is not formed with O_2), is active in the selective oxidation of CH_4 and benzene at room temperature.

O_2 treatment of Fe-zeolites does not result in the formation of active sites for selective oxidation of methane and benzene. Rather, activated O_2 species in Fe-zeolites catalyze the non-selective oxidation of hydrocarbons into CO_x and H_2O at elevated temperatures (typically at 400°C or higher). This is observed in the selective catalytic reduction (SCR) of NO (similar as in Cu and Co-zeolites). At moderate temperatures (typically between 250-350°C), O_2 is beneficial for the SCR of NO. O_2 and activated O_2 species have been suggested to: i) oxidize NO into NO_2 or adsorbed NO_y (with y=2,3) species, ii) reoxidize the TMI to its “proper” oxidation state for NO-NO_2 conversion and adsorption,[130-136] ii) remove carbonaceous deposits[137] and, iv) oxidize hydrocarbons into more reactive oxygenated surface intermediates for NO reduction.[138] At higher temperatures however, the presence of O_2 results in a decreased reduction of NO, resulting in the typically observed volcano shaped conversion curves. The combustion of the hydrocarbons with the activated oxygen species is more dominant at these

temperatures leaving less hydrocarbons for the reduction of NO_x.[40, 139, 140] Little is known, however, on the geometric and electronic structure of the intermediates involved in both the low and high temperature reactions.

4.3 Co and other first-row TMI-zeolites

Other first row transition metal ions, such as Ti, V, Cr and Mn have been reported to be active in either N_2O decomposition or selective oxidation reactions. Recently, the presence of an α-O site in Mn-ZSM-5 was suggested after N_2O treatment, similar to Fe-ZSM-5. This so called α-O results in the formation of an absorption band in the UV-vis spectra around 18 500 cm^{-1}, and was suggested to be involved in the N_2O decomposition in Mn-ZSM-5.[141] No reactivity towards hydrocarbons is thus far reported for this species and as is the case for Fe-ZSM-5, the α-O in Mn-ZSM-5 cannot be formed with O_2. Although Mn-zeolites have been reported to catalyze the selective oxidation of n-hexane with O_2, the role of the Mn sites is not in O_2 activation. The proposed role of Mn is rather to regulate the selective decomposition of the hexylhydroperoxo intermediate in this reaction.[142] Isomorphously substituted V, Cr and Ti zeolites and mesoporous materials were found to be active in the photocatalytic partial oxidation of hydrocarbons with O_2.[143, 144] Supported isolated vanadium oxides on SiO_2, TiO_2, Al_2O_3 or mesoporous materials are often investigated in the selective oxidation of CH_4 or methanol into formaldehyde with O_2 at temperature above 400°C.[145-151] Isomorphous substitution of Ti in the zeolite lattice, e.g. TS-1 zeolite, results in active catalysts for the liquid-phase catalytic oxidation of a variety of organic compounds with H_2O_2.

Co exchanged zeolites or Co incorporated in the lattice of AlPO's has often been reported to be active in the selective oxidation of linear alkanes by O_2.[152, 153] Co exchanged X, Y zeolite or the mesoporous silica MCM-41 have been found to be active in the epoxidation of styrene with molecular oxygen in the presence of *N*,*N*-dimethyl formamide (DMF).[154-156] A tentative reaction mechanism was proposed for the O_2 oxidation of α-pinene and the epoxidation of styrene by Co exchanged FAU.[155, 157] Activation of O_2 in the presence of DMF at the Co sites is suggested to occur via a tetrahedrally coordinated Co^{III}-superoxo complex, with a typical absorption band at 620 nm (16130 cm^{-1}) in the UV-vis absorption spectrum,[155] followed by the oxidative addition to the C=C double bond of styrene and α-pinene.

5. Conclusions

This Forum contribution has reviewed the coordination of Cu^{2+}, Fe^{3+} and Co^{2+} to surface oxygens in zeolites, as derived from spectroscopic and theoretical studies, the formation of activated oxygen species and their role in selective oxidation reactions. At low loadings, the coordination of the TMI is reasonably well understood. Cu^{2+} is found to coordinate in 6MR, distorting the ring in such a way as to obtain 4-fold coordination. In the case of Co^{2+}, it can have 3-5 fold coordination. The resulting site distortion depends on the amount of Al tetrahedra making up that site. Thus, a TMI in one crystallographic exchange site can have several spectroscopic signatures, depending on the number of Al tetrahedra. As a result, both the crystallographic position of the exchange site and the number of Al tetrahedra making up the site determine the spectroscopic signature and thus the geometric and electronic structure of the TMI in that site.

Increasing the TMI loading increases the heterogeneity of the TMI species formed at the zeolite surface. This can result in the formation of di- and oligomeric species, requiring extra-lattice ligands (water, hydroxo and oxo ligands). Removal of these ligands during high temperature pretreatments can result in auto-reduction of the TMI as confirmed by XANES and UV-vis studies. Several mechanisms for auto-reduction have been suggested. However decisive spectroscopic evidence for the proposed intermediates is lacking.

The reduced TMI sites possess interesting properties. At room temperature, O_2 is only weakly adsorbed in most zeolites, but superoxo complexes have been reported to be formed with Cu^+ and Cr^{2+} in zeolite A. High temperature treatment in O_2 leads to the formation a catalytically interesting core in Cu-ZSM-5, characterized by a distinct absorption band around 22 700 cm^{-1}. A recent resonance Raman studied allowed assignment of this active site as a bent $[Cu\text{-}O\text{-}Cu]^{2+}$ core.[101] This species, corresponding to only about 5% of the total amount of Cu, is the crucial intermediate in both the direct decomposition of NO and N_2O and the selective oxidation of methane into methanol in a stoichiometric reaction. Other Cu-zeolites, not containing this species, are also active in the selective oxidation of methane into methanol, but at higher temperature. Research is now directed toward: i) further understanding the electronic and geometric structure and reactivity of the bent $[Cu\text{-}O\text{-}Cu]^{2+}$ core in the oxygen-activated Cu-ZSM-5 ii) obtaining more information on active sites in other Cu-zeolites; iii) devising a catalytic cycle for the methane-to-methanol conversion with Cu and Fe–zeolites, and iv) increasing the number of active sites.

An activated oxygen species, called α-oxygen, is formed in Fe-ZSM-5. There is a lot of speculation as to the nature of this α-oxygen species. All involve mononuclear and binuclear Fe-oxo species. Its definitive spectroscopic characterization and assignment is also lacking. Consensus however does exist on its role in the selective oxidation of methane and benzene into methanol and phenol, respectively, at room temperature. The hydroxylation of benzene was converted in a catalytic system upon increasing the reaction temperature, favoring the desorption of phenol. In the reaction with CH_4, increasing the temperature results in the decomposition of methanol into CO_2 and H_2O, as is the case in O_2 activated Cu-ZSM-5. In contrast to Cu-ZSM-5 however, this reactive α-oxygen in Fe-ZSM-5 cannot be formed with O_2 (i.e. only with N_2O).

Treatment of Co-exchanged FAU with O_2 is suggested to result in the formation of a Co^{III}-superoxo complex in FAU zeolite based on an absorption band at 620 nm. This superoxo species is found to be active in the epoxidation of styrene and the oxidation of α-pinene. Additional spectroscopic studies are needed to obtain insight into this O_2-formed active Co^{III} site and the molecular mechanism of these reactions.

Overall, O_2 activation depends on the interplay of structural factors such as zeolite type, size of the channels and cages and chemical factors such as Si/Al ratio and nature, charge and distribution of the cations. Spectroscopic techniques capable of selectively probing the active sites, even though they constitute only a minor fraction of the total amount of TMI sites, are thus required. The fundamental knowledge of the active site obtained from such studies can provide detailed mechanistic insight and assist in the design and development of novel selective oxidation catalysts.

Acknowledgments

P.J.S. acknowledges the I.W.T. and K.U. Leuven for graduate and post-doctoral fellowships and J.S.W acknowledges the NIH for a traineeship. This research was supported by the G.O.A. and the Long Term Structural Funding-Methusalem Funding by the Flemish Government (R.A.S., B.F.S.) and NIH Grant DK-31450 (E.I.S.).

References

1. Breck, DW. Zeolite Molecular Sieves. Wiley & Sons; New York: 1974. p. 771
2. Shen DM, Bulow M, Siperstein F, Engelhard M, Myers AL. Adsorption 2000;6:275–286.
3. McKee, DW. US patent. US:3140933. 1964.
4. Yang RT, Chen YD, Peck JD, Chen N. Ind. Eng. Chem. Res 1996;35:3093–3099.
5. Dunne JA, Mariwals R, Rao M, Sircar S, Gorte RJ, Myers AL. Langmuir 1996;12:5888–5895.

6. Chao, CC. Eur. Patent. EP0,297,542,A2. 1983.
7. Jousse F, DeLara EC. J. Phys. Chem 1996;100:233–237.
8. Jousse F, Larin AV, DeLara EC. J. Phys. Chem 1996;100:238–244.
9. Xu J, Mojet BL, van Ommen JG, Lefferts L. J. Phys. Chem. B 2005;109:18361–18368. [PubMed: 16853364]
10. Santra S, Archipov TE, Augusta B, Komnik H, Stoll H, Roduner E, Rauhut G. Phys. Chem. Chem. Phys. 2009 DOI: 10.1039/b904152d.
11. Klier K. Langmuir 1988;4:13–25.
12. Kellerman R, Hutta PJ, Klier K. J. Am. Chem. Soc 1974;96:5946–5947.
13. Kellerman, R.; Klier, K. Molecular Sieves -II. Katzer, JR., editor. Vol. Vol. 40. American Chemical Society; Washington, DC: 1977. p. 120
14. Lange JP, Klier K. Zeolites 1994;14:462–468.
15. Vansant EF, Lunsford JH. J. Phys. Chem 1972;76:2860. &.
16. Lunsford J. ACS Symp. Ser 1977;40:473.
17. Schoonheydt RA, Pelgrims J. J. Chem. Soc., Dalton Trans 1981:914–922.
18. Devos DE, Knops-Gerrits PP, Parton RF, Weckhuysen BM, Jacobs PA, Schoonheydt RA. J.Incl. Phenom. Mol. Recognit. Chem 1995;21:185–213.
19. De Vos DE, Dams M, Sels BF, Jacobs PA. Chem. Rev 2002;102:3615–3640. [PubMed: 12371896]
20. Corma A, Garcia H. Chem. Rev 2002;102:3837–3892. [PubMed: 12371904]
21. Ratnasamy P, Srinivas D. Catal. Today 2009;141:3–11.
22. Corma A. Chem. Rev 1997;97:2373–2419. [PubMed: 11848903]
23. Punniyamurthy T, Velusamy S, Iqbal J. Chem. Rev 2005;105:2329–2363. [PubMed: 15941216]
24. Viswanathan B, Jacob B. Catal. Rev 2005;47:1–82.
25. van Bekkum, H.; Flanigen, E.; Jacobs, PA.; Jansen, JC. Introduction to Zeolite Science and Practice. 2nd ed. Elsevier; Amsterdam: 2001. p. 1018
26. Baerlocher, C.; McCusker, LB. Database of Zeolite Structures. http://www.iza-structure.org/databases/
27. Treacy, MMJ.; Higgins, JB. Collection of Simulated XRD Powder Patterns for Zeolites. 5th ed. Elsevier; Amsterdam: 2007.
28. Jacobs, PA.; Martens, JA.; van Bekkum, EMFH.; Jansen, JC. Studies in Surface Science and Catalysis. Vol. Vol. Volume 58. Elsevier; 1991. Introduction to Acid Catalysis with Zeolites in Hydrocarbon Reactions; p. 445-496.
29. Smeets PJ, Sels BF, van Teeffelen RM, Leeman H, Hensen EJM, Schoonheydt RA. J. Catal 2008;256:183–191.
30. De Vos DE, Sels BF, Jacobs PA. Adv. Catal 2001;46:1–87.
31. Notari, B. Innovation in Zeolite Materials Science. In: Grobet, PJ.; Mortier, WJ.; Vansant, EF.; Schulz-Ekloff, G., editors. Stud. Surf. Sci. Catal. Vol. Vol. 37. Elsevier; Amsterdam: 1988. p. 413
32. Clerici, MG.; Romano, U. Eur. Patent. EP100,119,A1. 1983.
33. Bellusi, G.; Giusti, A.; Esposito, A.; Buonomo, F. Eur. Patent. EP226,257,A2. 1987.
34. Pirngruber, G. The fascinating chemistry of iron- and copper-containing zeolites. In: Valtchev, V.; Mintova, S.; Tsapatsis, M., editors. Ordered Porous Materials. Elsevier; Amsterdam: 2008. p. 733
35. Mortier, WJ. Compilation of extra framework sites in zeolites. Butterworth Sci. Ltd.; Guildford: 1982. p. 67
36. Karge HG, Zhang Y, Beyer HK. Catal. Lett 1992;12:147–156.
37. Weitkamp, J.; Ernst, S.; Bock, T.; Kromminga, T.; Kiss, A.; Kleinschmit, P. US Patent. US:5545784. 1994.
38. Sulikowski B, Find J, Karge HG, Herein D. Zeolites 1997;19:395–403.
39. Iwamoto M, Yahiro H, Mine Y, Kagawa S. Chem. Lett 1989:213–216.
40. Smeets PJ, Meng QG, Corthals S, Leeman H, Schoonheydt RA. Appl. Catal. B 2008;84:505–513.
41. Wichterlova B, Dedecek J, Sobalik Z. Catalysis by Unique Metal Ion Structures in Solid Matrices: From Science to Application 2001;13:31–53.

42. Dedecek J, Wichterlova B. J. Phys. Chem. B 1999;103:1462–1476.
43. Kaucky D, Dedecek JI, Wichterlova B. Microporous Mesoporous Mat 1999;31:75–87.
44. Dedecek J, Kaucky D, Wichterlova B. Microporous Mesoporous Mat 2000;35-6:483–494.
45. Dedecek J, Kaucky D, Wichterlova B, Gonsiorova O. Phys. Chem. Chem. Phys 2002;4:5406–5413.
46. Drozdova L, Prins R, Dedecek J, Sobalik Z, Wichterlova B. J. Phys. Chem. B 2002;106:2240–2248.
47. Verberckmoes AA, Weckhuysen BM, Pelgrims J, Schoonheydt RA. J. Phys. Chem 1995;99:15222–15228.
48. Verberckmoes AA, Weckhuysen BM, Schoonheydt RA. Microporous Mesoporous Mat 1998;22:165–178.
49. Groothaert MH, Pierloot K, Delabie A, Schoonheydt RA. Phys. Chem. Chem. Phys 2003;5:2135–2144.
50. Schoonheydt RA. Catal. Rev 1993;35:129–168.
51. Pierloot, K.; Delabie, A.; Verberckmoes, A.; Schoonheydt, R. The Interplay between DFT and Conventional Quantum Chemistry: Coordination of Transition Metal Ions to Six-Rings in Zeolites. In: De Proft, F.; Langenaeker, W., editors. Density Functional Theory, a bridge between chemistry and physics Geerlings. VUB University Press; Brussels: 1999. p. 169
52. Pierloot K, Delabie A, Groothaert MH, Schoonheydt RA. Phys. Chem. Chem. Phys 2001;3:2174–2183.
53. Delabie A, Pierloot K, Groothaert MH, Weckhuysen BM, Schoonheydt RA. Phys. Chem. Chem. Phys 2002;4:134–145.
54. Delabie A, Pierloot K, Groothaert MH, Schoonheydt RA, Vanquickenborne LG. Eur. J. Inorg. Chem 2002:515–530.
55. Pierloot K, Delabie A, Ribbing C, Verberckmoes AA, Schoonheydt RA. J. Phys. Chem. B 1998;102:10789–10798.
56. Verberckmoes, A.; Schoonheydt, R.; Ceulemans, A.; Delabie, A.; Pierloot, K. Semi-emperical and ab-initio Calculations of the Spectroscopic properties of Co(II) coordinated in Zeolite A. In: Treacy, M.; Marcus, B.; Bisher, M.; Higgins, J., editors. Proceed. of the 12th International Zeolite Conference; Warrendale: Materials Research Society; 1999. p. 387
57. Klier, K.; Hutta, PJ.; Kellerman, R. In Molecular Sieves -II. Katzer, JR., editor. Vol. Vol. 40. American Chemical Society; Washington, DC: 1977. p. 108
58. Klier, K. Electronic structure of transition-metal ion containing zeolites. In: Centi, G.; Bell, AT.; Wichterlova, B., editors. Catalysis by Unique Metal Structures in Solid Matrices– From Science to Applications. Kluwer Academic Press; Dordrecht: 2001. p. 115
59. Schoonheydt RA. J. Phys. Chem. Solids 1989;50:523–539.
60. Perez-Ramirez J, Mul G, Kapteijn F, Moulijn JA, Overweg AR, Domenech A, Ribera A, Arends I. J. Catal 2002;207:113–126.
61. Zecchina A, Rivallan M, Berlier G, Lamberti C, Ricchiardi G. Phys. Chem. Chem. Phys 2007;9:3483–3499. [PubMed: 17612716]
62. Lobree LJ, Hwang IC, Reimer JA, Bell AT. J. Catal 1999;186:242–253.
63. Joyner R, Stockenhuber M. J. Phys. Chem. B 1999;103:5963–5976.
64. Heijboer WM, Battiston AA, Knop-Gericke A, Havecker M, Mayer R, Bluhm H, Schlogl R, Weckhuysen BM, Koningsberger DC, de Groot FMF. J. Phys. Chem. B 2003;107:13069–13075.
65. Battiston AA, Bitter JH, de Groot FMF, Overweg AR, Stephan O, van Bokhoven JA, Kooyman PJ, van der Spek C, Vanko G, Koningsberger DC. J. Catal 2003;213:251–271.
66. Marturano P, Drozdova L, Pirngruber GD, Kogelbauer A, Prins R. Phys. Chem. Chem. Phys 2001;3:5585–5595.
67. Heijboer WM, Battiston AA, Knop-Gericke A, Havecker M, Bluhm H, Weckhuysen BM, Koningsberger DC, de Groot FMF. Phys. Chem. Chem. Phys 2003;5:4484–4491.
68. Garten RL, Delgass WN, Boudart M. J. Catal 1970;18:90–107.
69. Larsen SC, Aylor A, Bell AT, Reimer JA. J. Phys. Chem 1994;98:11533–11540.
70. Iwamoto M, Yahiro H, Tanda K, Mizuno N, Mine Y, Kagawa S. J. Phys. Chem 1991;95:3727–3730.
71. Jacobs PA, Beyer HK. J. Phys. Chem 1979;83:1174–1177.

72. Groothaert MH, van Bokhoven JA, Battiston AA, Weckhuysen BM, Schoonheydt RA. J. Am. Chem. Soc 2003;125:7629–7640. [PubMed: 12812505]
73. Kau LS, Spirasolomon DJ, Pennerhahn JE, Hodgson KO, Solomon EI. J. Am. Chem. Soc 1987;109:6433–6442.
74. Nachtigallova D, Nachtigall P, Sierka M, Sauer J. Phys. Chem. Chem. Phys 1999;1:2019–2026.
75. Nachtigall P, Nachtigallova D, Sauer J. J. Phys. Chem. B 2000;104:1738–1745.
76. Nachtigallova D, Nachtigall P, Sauer J. Phys. Chem. Chem. Phys 2001;3:1552–1559.
77. Groothaert MH, Lievens K, Leeman H, Weckhuysen BM, Schoonheydt RA. J. Catal 2003;220:500–512.
78. Dandekar A, Vannice MA. Appl. Catal. B 1999;22:179–200.
79. Kapteijn F, Marban G, RodriguezMirasol J, Moulijn JA. J. Catal 1997;167:256–265.
80. Smeets PJ, Groothaert MH, van Teeffelen RM, Leeman H, Hensen EJM, Schoonheydt RA. J. Catal 2007;245:358–368.
81. Groothaert MH, Smeets PJ, Sels BF, Jacobs PA, Schoonheydt RA. J. Am. Chem. Soc 2005;127:1394–1395. [PubMed: 15686370]
82. Smeets PJ, Groothaert MH, Schoonheydt RA. Catal. Today 2005;110:303–309.
83. Tyeklar Z, Jacobson RR, Wei N, Murthy NN, Zubieta J, Karlin KD. J. Am. Chem. Soc 1993;115:2677–2689.
84. Baldwin MJ, Ross PK, Pate JE, Tyeklar Z, Karlin KD, Solomon EI. J. Am. Chem. Soc 1991;113:8671–8679.
85. Baldwin MJ, Root DE, Pate JE, Fujisawa K, Kitajima N, Solomon EI. J. Am. Chem. Soc 1992;114:10421–10431.
86. Mahapatra S, Halfen JA, Wilkinson EC, Pan GF, Cramer CJ, Que L, Tolman WB. J. Am. Chem. Soc 1995;117:8865–8866.
87. Root DE, Mahroof-Tahir M, Karlin KD, Solomon EI. Inorg. Chem 1998;37:4838–4848. [PubMed: 11670647]
88. Chen P, Fujisawa K, Solomon EI. J. Am. Chem. Soc 2000;122:10177–10193.
89. Chen P, Root DE, Campochiaro C, Fujisawa K, Solomon EI. J. Am. Chem. Soc 2003;125:466–474. [PubMed: 12517160]
90. Maiti D, Fry HC, Woertink JS, Vance MA, Solomon EI, Karlin KD. J. Am. Chem. Soc 2007;129:264–265. [PubMed: 17212392]
91. Yumura T, Takeuchi M, Kobayashi H, Kuroda Y. Inorg. Chem 2009;48:508–517. [PubMed: 19093853]
92. Rice MJ, Chakraborty AK, Bell AT. J. Phys. Chem. B 2000;104:9987–9992.
93. Goodman BR, Schneider WF, Hass KC, Adams JB. Catal. Lett 1998;56:183–188.
94. Goodman BR, Hass KC, Schneider WF, Adams JB. J. Phys. Chem. B 1999;103:10452–10460.
95. Iwamoto M, Furukawa H, Mine Y, Uemura F, Mikuriya SI, Kagawa S. J. Chem Soc. Chem. Commun 1986:1272–1273.
96. Sarkany J, Ditri JL, Sachtler WMH. Catal. Lett 1992;16:241–249.
97. Da Costa P, Moden B, Meitzner GD, Lee DK, Iglesia E. Phys. Chem. Chem. Phys 2002;4:4590–4601.
98. Palomino GT, Fisicaro P, Bordiga S, Zecchina A, Giamello E, Lamberti C. J. Phys. Chem. B 2000;104:4064–4073.
99. Xamena F, Fisicaro P, Berlier G, Zecchina A, Palomino GT, Prestipino C, Bordiga S, Giamello E, Lamberti C. J. Phys. Chem. B 2003;107:7036–7044.
100. Grunert W, Hayes NW, Joyner RW, Shpiro ES, Siddiqui MRH, Baeva GN. J. Phys. Chem 1994;98:10832–10846.
101. Woertink JS, Smeets PJ, Groothaert MH, Vance MA, Sels BF, Schoonheydt RA, Solomon EI. Proc. Natl. Acad. Sci. USA 2009;106:18908–18913. [PubMed: 19864626]
102. Panov GI, Sobolev VI, Kharitonov AS. J. Mol. Catal 1990;61:85–97.
103. Panov GI, Sheveleva GA, Kharitonov AS, Romannikov VN, Vostrikova LA. Appl. Catal. A 1992;82:31–36.

104. Sobolev VI, Kharitonov AS, Paukshtis YA, Panov GI. J. Mol. Catal 1993;84:117–124.
105. Dubkov KA, Sobolev VI, Talsi EP, Rodkin MA, Watkins NH, Shteinman AA, Panov GI. J. Mol. Catal. A 1997;123:155–161.
106. Dubkov KA, Sobolev VI, Panov GI. Kinet. Catal 1998;39:72–79.
107. Ovanesyan NS, Shteinman AA, Dubkov KA, Sobolev VI, Panov GI. Kinet. Catal 1998;39:792–797.
108. Kubanek P, Wichterlova B, Sobalik Z. J. Catal 2002;211:109–118.
109. Ribera A, Arends I, de Vries S, Perez-Ramirez J, Sheldon RA. J. Catal 2000;195:287–297.
110. Knops-Gerrits PP, Goddard WA. J. Mol. Catal. A 2001;166:135–145.
111. Hensen EJM, Zhu Q, Hendrix M, Overweg AR, Kooyman PJ, Sychev MV, van Santen RA. J. Catal 2004;221:560–574.
112. Sun KQ, Zhang HD, Xia H, Lian YX, Li Y, Feng ZC, Ying PL, Li C. Chem. Commun 2004:2480–2481.
113. Dubkov KA, Ovanesyan NS, Shteinman AA, Starokon EV, Panov GI. J. Catal 2002;207:341–352.
114. Ivanov AA, Chernyavsky VS, Gross MJ, Kharitonov AS, Uriarte AK, Panov GI. Appl. Catal. A 2003;249:327–343.
115. Yuranov I, Bulushev DA, Renken A, Kiwi-Minsker L. J. Catal 2004;227:138–147.
116. Roy PK, Pirngruber GD. J. Catal 2004;227:164–174.
117. Ovanesyan NS, Sobolev VI, Dubkov KA, Panov GI, Shteinman AA. Russ. Chem. Bull 1996;45:1509–1510.
118. Shilov AE, Shteinman AA. Accounts of Chemical Research 1999;32:763–771.
119. Jia JF, Sun Q, Wen B, Chen LX, Sachtler WMH. Catal. Lett 2002;82:7–11.
120. Pirngruber GD, Grunwaldt JD, van Bokhoven JA, Kalytta A, Reller A, Safonova OV, Glatzel P. J. Phys. Chem. B 2006;110:18104–18107. [PubMed: 16970419]
121. Pirngruber GD, Grunwaldt JD, Roy PK, van Bokhoven JA, Safonova O, Glatzel P. Catal. Today 2007;126:127–134.
122. Berrier E, Ovsitser O, Kondratenko EV, Schwidder M, Grunert W, Bruckner A. J. Catal 2007;249:67–78.
123. Neidig ML, Decker A, Choroba OW, Huang F, Kavana M, Moran GR, Spencer JB, Solomon EI. Proc. Natl. Acad. Sci. USA 2006;103:12966–12973. [PubMed: 16920789]
124. Solomon EI, Wong SD, Liu LV, Decker A, Chow MS. Curr. Opin. Chem. Biol 2009;13:99–113. [PubMed: 19278895]
125. Krzystek J, England J, Ray K, Ozarowski A, Smirnov D, Que L, Telser J. Inorg. Chem 2008;47:3483–3485. [PubMed: 18386920]
126. Pirngruber GD, Roy PK, Prins R. Phys. Chem. Chem. Phys 2006;8:3939–3950. [PubMed: 17028684]
127. Xia HA, Sun KQ, Sun KJ, Feng ZC, Li WX, Li C. J. Phys. Chem. C 2008;112:9001–9005.
128. Gao ZX, Kim HS, Sun Q, Stair PC, Sachtler WMH. J. Phys. Chem. B 2001;105:6186–6190.
129. Capek L, Kreibich V, Dedecek J, Grygar T, Wichterlova B, Sobalik Z, Martens JA, Brosius R, Tokarova V. Microporous Mesoporous Mat 2005;80:279–289.
130. Hamada H, Kintaichi Y, Sasaki M, Ito T, Tabata M. Appl. Catal 1991;70:L15–L20.
131. Komatsu T, Nunokawa M, Moon IS, Takahara T, Namba S, Yashima T. J. Catal 1994;148:427–437.
132. Ham SW, Choi H, Nam IS, Kim YG. Catal. Lett 1996;42:35–40.
133. Eng J, Bartholomew CH. J. Catal 1997;171:27–44.
134. Schay Z, James VS, Pal-Borbely G, Beck A, Ramaswamy AV, Guczi L. J. Mol. Catal. A 2000;162:191–198.
135. Delahay R, Kieger S, Tanchoux N, Trens P, Coq B. Appl. Catal. B 2004;52:251–257.
136. Sjovall H, Olsson L, Fridell E, Blint R. J. Appl. Catal. B 2006;64:180–188.
137. d'Itri JL, Sachtler WMH. Appl. Catal. B 1993;2:L7–L15.
138. Montreuil CN, Shelef M. Appl. Catal. B 1992;1:L1–L8.
139. Chen HY, Voskoboinikov T, Sachtler WMH. J. Catal 1999;186:91–99.

140. Parvulescu VI, Grange P, Delmon B. Catal. Today 1998;46:233–316.
141. Radu D, Glatzel P, Gloter A, Stephan O, Weckhuysen BM, de Groot FMF. J. Phys. Chem. C 2008;112:12409–12416.
142. Zhan BZ, Moden B, Dakka J, Santiesteban JG, Iglesia E. J. Catal 2007;245:316–325.
143. Anpo M, Kim TH, Matsuoka M. Catal. Today 2009;142:114–124.
144. Hu Y, Wada N, Tsujimaru K, Anpo M. Catal. Today 2007;120:139–144.
145. Herman RG, Sun Q, Shi CL, Klier K, Wang CB, Hu HC, Wachs IE, Bhasin MM. Catal. Today 1997;37:1–14.
146. Bronkema JL, Bell AT. J. Phys. Chem. C 2007;111:420–430.
147. Berndt H, Martin A, Bruckner A, Schreier E, Muller D, Kosslick H, Wolf GU, Lucke B. J. Catal 2000;191:384–400.
148. Koranne MM, Goodwin JG, Marcelin G. J. Catal 1994;148:378–387.
149. Parmaliana A, Arena F. J. Catal 1997;167:57–65.
150. Baltes M, Cassiers K, Van Der Voort P, Weckhuysen BM, Schoonheydt RA, Vansant EF. J. Catal 2001;197:160–171.
151. Deo G, Wachs IE. J. Catal 1994;146:323–334.
152. Thomas JM, Raja R, Sankar G, Bell RG. Nature 1999;398:227–230.
153. Thomas JM. Angew. Chem. Int. Ed 1999;38:3589–3628.
154. Tang QH, Wang Y, Liang J, Wang P, Zhang QH, Wan HL. Chem. Commun 2004:440–441.
155. Sebastian J, Jinka KM, Jasra RV. J. Catal 2006;244:208–218.
156. Tang QH, Zhang QH, Wu HL, Wang Y. J. Catal 2005;230:384–397.
157. Patil MV, Yadav MK, Jasra RV. J. Mol. Catal. A 2007;277:72–80.

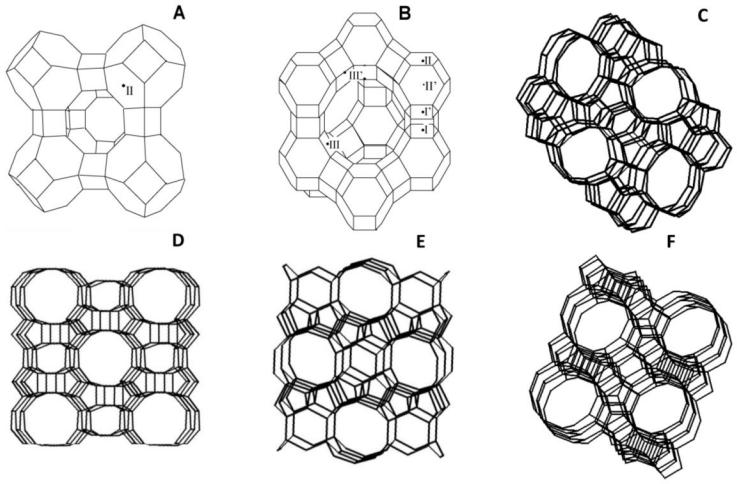

Figure 1.
Industrially most important zeolite structures: A) LTA, B) X and Y (FAU topology), C) ZSM-5 (MFI topology), D) MOR, E) FER and F) *BEA. The symbols I, I′, II, II′, III, and III′ indicate exchangeable cation sites in LTA and FAU. The lines represent the O atoms; the corners Si or Al atoms. ZSM-5, MOR and FER are also known as pentasil zeolites.

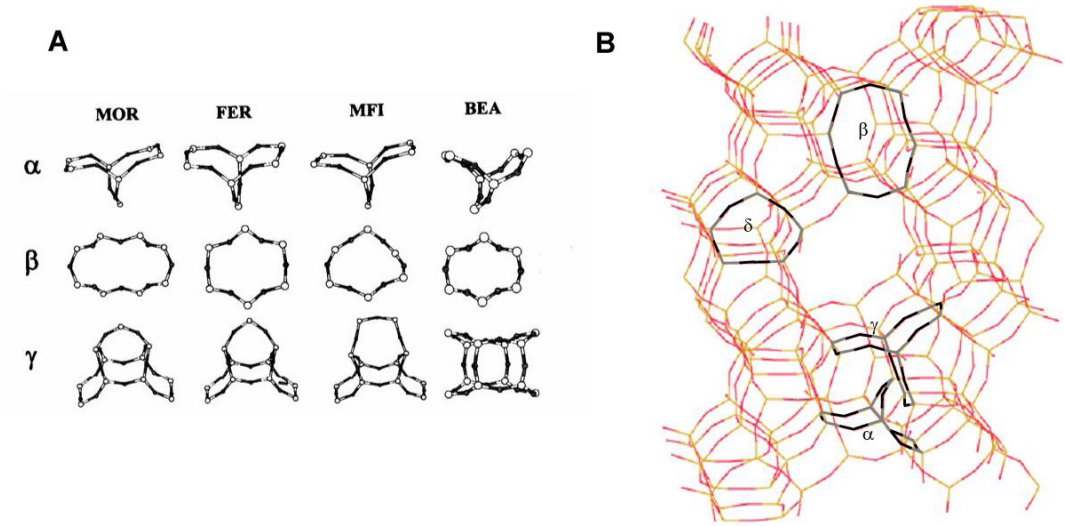

Figure 2.
A) Local framework structures of α, β and γ sites in the MOR, ferrierite (FER), MFI and Beta (*BEA) zeolites.[41] B) crystallographic position of these sites in ZSM-5.[49] Reproduced by permission of the PCCP Owner Societies.

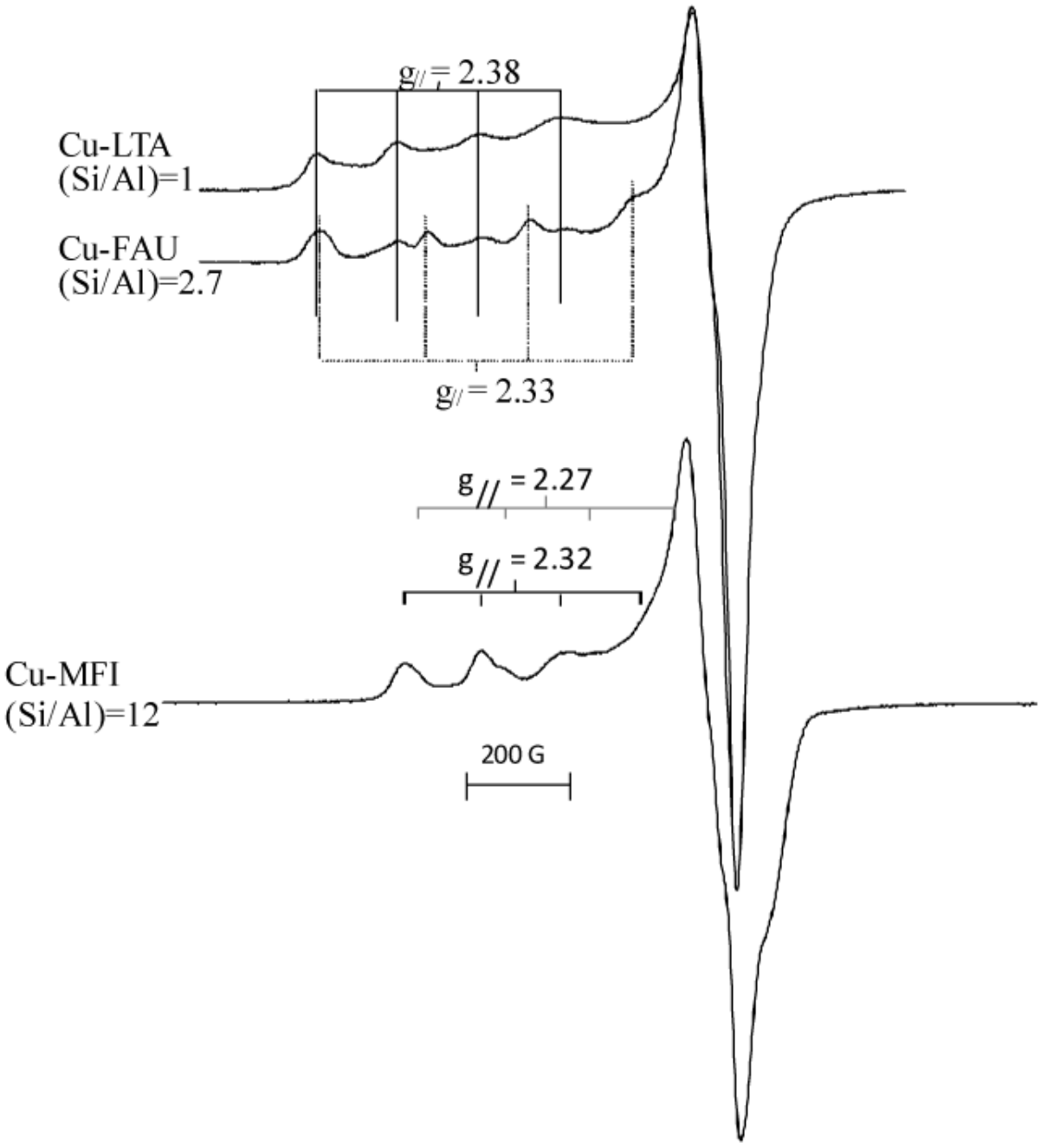

Figure 3.
Typical EPR spectra of Cu^{2+}-LTA, Cu^{2+}-FAU and Cu^{2+}-MFI after dehydration in O_2 at 450° C.

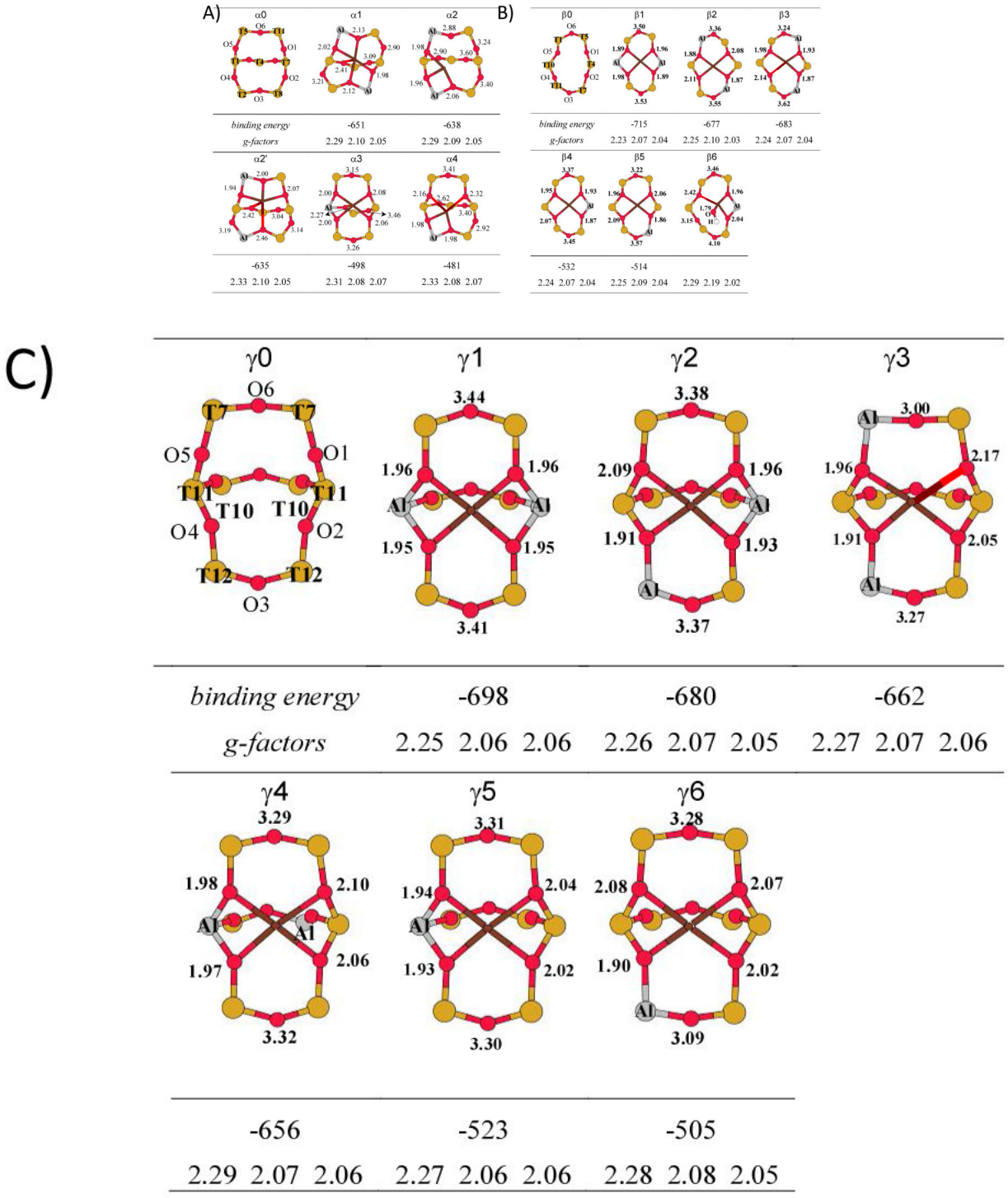

Figure 4.

The optimized Cu(II) coordination (brown) in the α (A), β (B) and γ (C) sites of ZSM-5 containing 1 or 2 lattice Al T-sites. The corresponding Cu-O distances (Å), Cu(II) binding energies (kcal mol^{-1}) and g-factors of the distorted sites are given. The Cu(II) free sites are shown as α0, β0 and γ0. [49] Reproduced by permission of the PCCP Owner Societies.

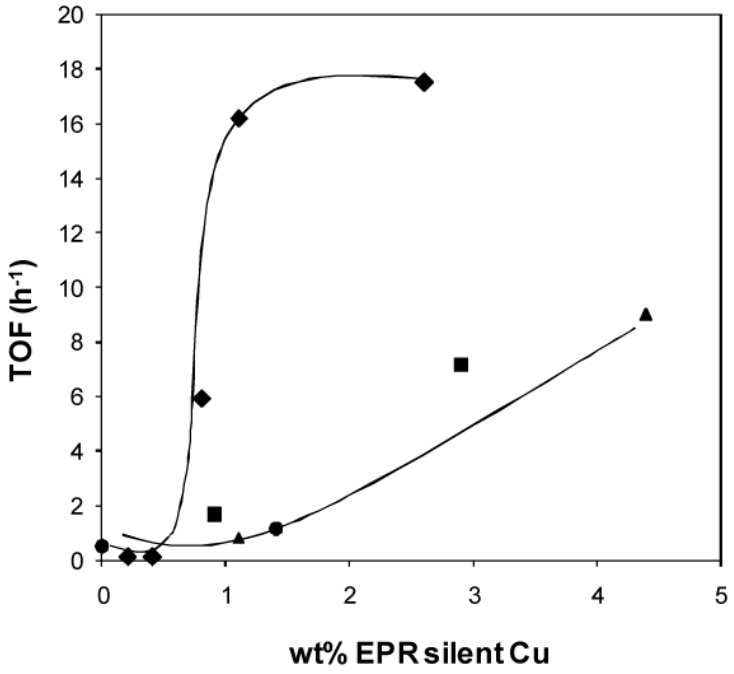

Figure 5.
Activity per Cu (TOF) for N_2O decomposition as a function of the EPR silent Cu^{2+} in (◆) Cu-ZSM-5 (Si/Al=12) (▲) Cu-MOR (Si/Al=8.8), (•) Cu-BEA (Si/Al=9.8)and (■) Cu-FER (Si/Al=6.2). Reprinted from [80] with permission from Elsevier.

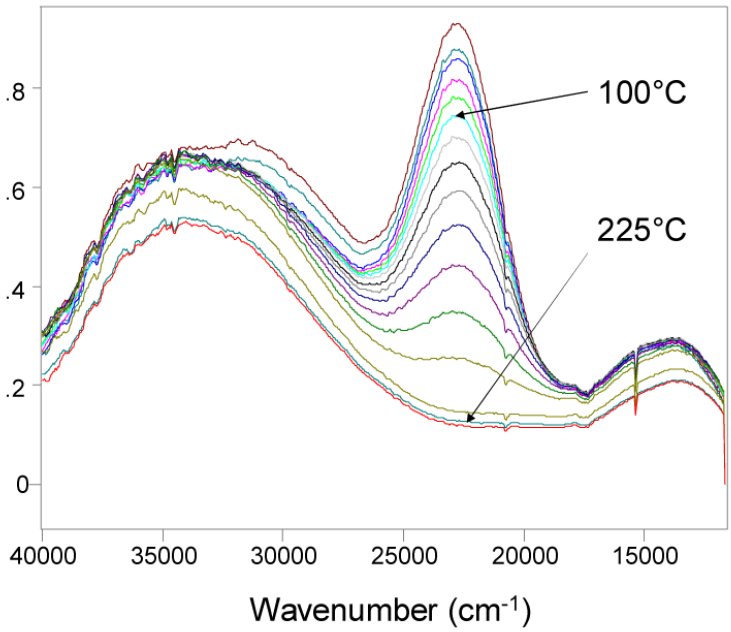

Figure 6.
Fiber-optic UV–vis spectra of an O_2 calcined (450°C) Cu-ZSM-5 (Si/Al=12, Cu/Al=0.54) during reaction with CH_4 at a heating rate of 10 °C/min from RT up to 225 °C. The time interval between two spectra is 1.5 min or a temperature difference of 15 °C. Reprinted from [82] with permission from Elsevier.

Table 1

Pore sizes, typical unit cell compositions and dimensionality of the channel systems of LTA, FAU MFI, MOR, FER and *BEA.[26]

Zeolite topology	Pore sizes (Å)	Unit cell	Channel system
LTA	8-ring: 4.1 × 4.1	$\|Na^{+}_{12}\,(H_2O)_m\|\,[Al_{12}Si_{12}\,O_{48}]$	3-dimensional
FAU	12-ring: 7.4 × 7.4	$(Ca^{2+}Mg^{2+}Na^{+}_{2})_{29}\,(H_2O)_m\|\,[Al_{58}Si_{134}\,O_{384}]$	3-dimensional
MFI	10-ring: 5.1 × 5.5 10-ring: 5.3 × 5.6	$\|Na^{+}_{n}\,(H_2O)_m\|\,[Al_nSi_{96-n}\,O_{192}]$	3-dimensional
MOR	12-ring: 6.5 × 7.0 8-ring: 2.6 × 5.7	$\|Na^{+}_{8}\,(H_2O)_m\|\,[Al_8Si_40\,O_{96}]$	1-dimensional
FER	10-ring: 4.2 × 5.4 8-ring: 3.5 × 4.8	$\|Mg^{2+}_{2}Na^{+}_{2}\,(H_2O)_m\|\,[Al_6Si_{30}\,O_{72}]$-	2-dimensional
*BEA	12-ring: 6.6 × 6.7 12-ring: 5.6 × 5.6	$\|Na^{+}_{7}(H_2O)_m\,\|\,[Al_7Si_{57}\,O_{128}]$	3-dimensional

Table 2

d-d transitions of Co^{2+} occupying α, β and γ sites in the pentasil zeolites and *BEA.[42-44, 46]

Zeolite	Energy (cm−1)		
Site:	**α**	**β**	**γ**
MFI	15 100	16 000, 17 150, 18600, 21 200	20 100, 22 000
MOR	14 800	15 900, 17 500, 19 200, 21 100	20 150, 22 050
FER	15 000	16 000, 17 100, 18 700, 20 600	20 300, 22 000
*BEA	14 600	15 500, 16 300, 17 570, 21 700	18 900, 22 060

Table 3

d-d transitions and EPR parameters of Cu^{2+} coordinated to six-membered oxygen rings in zeolites after dehydration (O_2 at 450°C).[54, 59]

zeolite	d-d transitions (cm^{-1})	$g_{\|\|}$	$A_{\|\|} \times 10^{-4}$ cm^{-1}	$g_{\perp}$	$A_{\perp} \times 10^{-4}$ cm^{-1}
LTA	10500, 12200,15100	2.37-2.41	130-145	2.06-2.07	19
FAU	10300-10700, 12600,15000	2.36-2.41	120-145	2.06-2.08	19
		2.30-2.34	171-188	2.05-2.07	19
MOR, MFI	14000(broad)	2.30-2.33	156-180	2.04-2.07	3-25
		2.26-2.28	168-192	2.05-2.07	3-25